Formal upscaling and numerical validation of fractured flow models for Richards′ equation

K. Kumar, F. List, I.S. Pop, F.A. Radu

UHasselt Computational Mathematics Preprint
Nr. UP-19-03

March 1, 2019

Formal upscaling and numerical validation of fractured flow models for Richards' equation

Kundan Kumar[a,b,*], Florian List[c,d], Iuliu Sorin Pop[c], Florin Adrian Radu[b]

[a] *Department of Mathematics, Karlstad University, Sweden*
[b] *Department of Mathematics, University of Bergen, Allegaten 41 Postboks 7803, 5020 Bergen, Norway*
[c] *Department of Mathematics, University of Hasselt, Belgium*
[d] *School of Physics, University of Sydney, Australia*

Abstract

In this work, we consider a mathematical model for describing flow in an unsaturated porous medium containing a fracture. Both the flow in the fracture as well as in the matrix blocks are governed by Richards' equation coupled by natural transmission conditions. Using formal asymptotics, we derive upscaled models as the vanishing limit of ε, the ratio of the width and length of the fracture. Our results show that the ratio of porosities and permeabilities in the fracture to matrix determine, to the leading order of approximation, the appropriate effective model. In these models the fracture is a lower dimensional object for which different transversally averaged models are derived depending on the ratio of the porosities and permeabilities of the fracture and respective matrix blocks. We obtain a catalogue of effective models which are validated by numerical computations.

Keywords: Richards' equation, Fractured porous media, Upscaling, Unsaturated flow in porous media,
35B27, 35A35, 35J25, 35K65

1. Introduction

Accounting for fractures in a porous medium has been a subject of great interest due to its wide applications in energy and environmental fields. For example, in the oil industry, fractures may enhance oil production. On the contrary in carbon sequestration, they may act as a leakage pathway. A fracture is a thin but long domain embedded in a porous matrix. Its hydraulic properties such as permeabilities may be drastically different from the matrix and its influence on the flow behaviour is quite strong [1], for example a highly permeable fracture network may provide the dominant pathway for

*Corresponding author: florian.list@uhasselt.be
Email addresses: kundan.kumar@uib.no (Kundan Kumar), sorin.pop@uhasselt.be (Iuliu Sorin Pop), florin.radu@uib.no (Florin Adrian Radu)

the entire flow in a porous medium. Therefore, fractures or entire fracture networks must be incorporated in the mathematical models for fluid flow. This is challenging from the numerical point of view, firstly due to the high geometrical complexity of fracture networks and secondly, a small aperture to length ratio makes it difficult to resolve the flow behaviour explicitly through brute force computations.

At the Darcy scale individual fractures look like a plane discontinuity. Viewed from a close up this thin region is composed of a porous medium though having markedly different properties from the matrix. To avoid a brute force computation involving fine scale resolution for the fracture domain, it is appealing to embed fractures as lower-dimensional manifolds into a higher-dimensional domain (e.g., as lines in a two-dimensional domain). Thus, a mathematical description of the flow consists of flow equations in the matrix block coupled to a differential equation on the lower-dimensional fracture surface. Depending on the hydraulic properties of the fractures with respect to the matrix, fractures may block or conduct fluid flow. This suggests that the effective model should distinguish between these two extreme cases. This is the subject matter of this paper. Herein, we show that there is a variety of models, each appropriate in a particular range for hydraulic properties of the fracture, that describe an effective behaviour of the flow in a fractured medium. Our approach yields these models beginning with a positive fracture width in the limit case where the width passes to zero. The presented model in this work provides a physically-consistent basis for discrete fracture modeling approaches (e.g. [15, 54]).

We consider a two-dimensional model for unsaturated fluid flow in a fractured porous medium. For the ease of presentation, the geometry is given by two rectangular matrix blocks, separated by a single fracture. We assume that the pore space of the porous medium is filled with a liquid (say water) and air. Provided that the domain is interconnected and connected to the surface, the assumption that the flow in air is infinitely mobile is justified, and the air pressure can be set to zero in the full two-phase model. We model the flow in both the matrix blocks and the fracture with Richards' equation, implying that the fracture consists of a porous medium as well (e.g. sediment-filled fractures [28], layered porous media [40]). This yields Richards' equation for the liquid phase

$$\partial_t(\phi S(\psi)) - \nabla \cdot (K_a K(S(\psi))\nabla\psi) = f, \tag{1}$$

as proposed by L. A. Richards in 1931 [49].
Here, ψ denotes the pressure head, ϕ is porosity of the medium, S is the water saturation, K_a and K stand for the absolute and relative hydraulic conductivity, respectively, and f is a source or sink term. The water saturation S is a given function of ψ, and the relative hydraulic conductivity is parametrised as a function of saturation, hence $K = K(S(\psi))$. The absolute hydraulic conductivity K_a depends on the soil properties. For anisotropic media, it is given as a matrix and may in general be a function of time and spatial co-ordinates. For the ease of notation, we assume K_a is a scalar constant in each subdomain herein. Note however that the extension of our results to anisotropic media is straightforward. For simplicity, the gravity is here neglected, but all the results of this paper can be extended to include it.

Based on experiments, various relationships have been proposed for the $S - \psi$ and $K - S$ dependencies (see e.g. [26]). Some of the popular ones include van Genuchten–

Mualem and Brooks–Corey [22, 26]. The parametrisation of the hydraulic relationships for the fracture may differ from the one for the matrix blocks, describing different materials in the fracture and the matrix blocks. Richards' equation is a degenerate parabolic equation, and its solution typically lacks regularity. Since our approach is formal, we make generous assumptions on the regularity of the solutions. This excludes the degenerate cases and assumes smoothness for all the solutions. We refer to [36] where mathematically rigorous convergence results are obtained for a certain range of parameters. For readers interested in the results concerning the existence of weak solutions including the degenerate cases, we refer to [4, 14], and for uniqueness results we mention e.g. [43].

Without aiming to be exhaustive, but for the sake of completeness we mention work being done for the numerical discretisation of Richards' equation and for the fractured media. Given the low regularity of the solution, and for stability reasons the implicit Euler scheme is commonly used for the time discretisation [45]. On the other hand, there are several techniques used for the spatial discretisation. We mention [18, 19, 30] for finite volume approaches, [6, 48, 57] for mixed finite element methods, and [16, 42] for continuous or discontinuous Galerkin methods. The implicit discretization leads to a system of non-linear algebraic equations that is typically solved using Newton approach or a combination of linearisation and Newton approach [13, 29]. For comparisons of different linearisation methods, we refer to [35]. Related to this context, since the medium consists of different homogeneous blocks, domain decomposition methods are quite appropriate. We refer to [10, 20] for a scheme using the mortar technique [7, 46] and to [53] for a linear domain decomposition scheme building on the schemes in [33] (see also [2, 8]). Some of the important works in the numerical methods for solving multiphase flow in fractured media include [21, 27, 31, 47, 50]. Concerning multiphysics extensions to fractured media that include mechanics we mention [56] for a phase field model describing the propagation of fluid filled fractures and [23, 24] for static fractures. For a recent review of current discretisation and modelling approaches used for flow in fractured media, we refer to [9] and references within. For the dimensional reduction of the fractures to interfaces, we refer to the works of [11, 20, 37, 38, 39]. For reactive flow upscaling in fractured medium we refer to [5, 17, 44].

This paper has two objectives: first, we derive effective models for the full range of permeability and porosity scaling ($\kappa \geq -1, \lambda \in \mathbb{R}$). Secondly, we show through numerical computations the validity of the effective models. The resulting model has a fracture as a one-dimensional line separating the two matrix blocks commonly referred to as mixed dimensional models. Letting ε stand for the ratio of width and the length of the fracture, depending on the scaling of the hydraulic conductivity and the porosity with respect to the ε, different effective models can arise. For example, if the fracture acts as a fault zone with low permeability, it will block the flow from the matrix. The fracture pressure then becomes irrelevant and a no-flow boundary condition for the matrix equations would describe this. In contrast, the fracture can become more permeable than the adjacent blocks becoming a preferential flow path. Accordingly, the equation for the fracture in the effective model can be an interface condition or a differential equation. Deriving such discrete fracture-matrix models has attracted quite a lot of attention recently. Relevant to our work is the formal derivation of fracture flow models for single phase, and two-phase flow models given in [3, 37]. However, our

approach is different and we make a comparison with existing approaches in Section 3.2. In contrast to a formal approach here, a rigorous mathematical approach has been pursued in [36, 38, 39, 44, 55] which deal with single phase flow for a highly permeable fracture that corresponds to a particular choice of scalings κ, λ. In [36] rigorous mathematical convergence results were obtained for the same model but for a restricted range of parameters. Because of the formal approach, here we are able to obtain the upscaled model in a wide regime ($\kappa > -1, \lambda \in \mathbb{R}$). Accordingly, we obtain a catalogue of upscaled models for each considered case, and their domain of validity for the permeability and porosity values. An extra motivation to pursue this formal approach is that it allows treating more complex models where one does not have the a priori estimates to justify the rigorous upscaling. Finally, we remark that only a single planar fracture in a two-dimensional case is considered. The extension to three dimensions is straightforward. Extending to a non-planar fracture is more technical as we have to use the differential geometry framework in order to define surface derivatives and will involve curvature terms.

The outline and approach of this work are as follows: in Section 2, the coupled model is formulated in a non-dimensional form, which will be used for the upscaling where we make an ansatz for the unknown variables as an expansion. Scaling parameters κ and λ are introduced, which account for the scaling of the porosities and hydraulic conductivities with respect to the fracture width. In Section 3, we provide a variety of effective equations depending on the parameters. Section 4 discusses the formal asymptotic expansion for the unknown variable and we obtain the effective equations. This asymptotic expansion is used to reduce the dimensionality of the fracture. Section 5 presents numerical simulations that show the validity of the upscaled models.

2. Model equations and scaling

We formulate the model directly in a dimensionless form. By relating the dimensional quantities to the reference quantities, the non-dimensional model is derived. For more details on the non-dimensionalisation, we refer to our paper [36] and to [34].

2.1. Model equations in dimensionless form

We resort to a simple two-dimensional geometry consisting of two square solid matrix blocks with edge length 1 separated by a fracture of width ε. The geometry is illustrated in Figure 1.

We assume that the porous medium Ω contains a subset Ω_f representing a single fracture. This divides the flow domain into two disjoint connected matrix subdomains $\Omega_{m_1}, \Omega_{m_2}$. The subscripts m and f indicate the matrix blocks and the fracture, respectively. They are defined as

$$\begin{aligned} \Omega_{m_1} &:= \left(-\frac{1}{2} - \frac{\varepsilon}{2}, -\frac{\varepsilon}{2}\right) \times (0,1), & \Gamma_1 &:= \left\{-\frac{\varepsilon}{2}\right\} \times (0,1), \\ \Omega_{m_2} &:= \left(\frac{\varepsilon}{2}, \frac{1}{2} + \frac{\varepsilon}{2}\right) \times (0,1), & \Gamma_2 &:= \left\{\frac{\varepsilon}{2}\right\} \times (0,1), \\ \Omega_f &:= \left(-\frac{\varepsilon}{2}, \frac{\varepsilon}{2}\right) \times (0,1). \end{aligned} \tag{2}$$

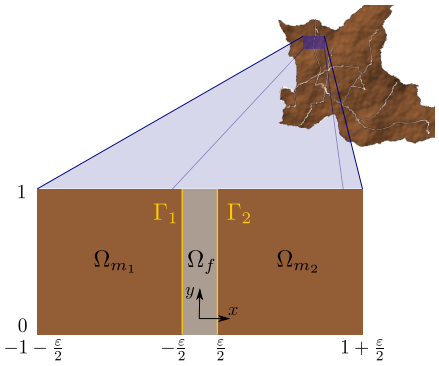

Figure 1: Dimensionless geometry of the fracture and the surrounding matrix blocks

Here $\Omega_m := \Omega_{m_1} \cup \Omega_{m_2}$ and $\Gamma_j,\ j = 1, 2$ are the interfaces separating fracture domain Ω_f and matrix block Ω_{m_j}. we set $\Omega^T := \Omega \times (0, T]$ for all spatial domains Ω and a given final time $T > 0$. Furthermore, $\vec{n}$ is a normal vector pointing from Ω_{m_j} into Ω_f. Note that in this dimensionless setting ε is the ratio of width to length of the fracture.

Richards' equation in the dimensionless form for the matrix blocks reads,

$$\partial_t S_m(\psi^\varepsilon_{m_j}) - \nabla \cdot \left(K_m(S_m(\psi^\varepsilon_{m_j}))\nabla\psi^\varepsilon_{m_j}\right) = f^\varepsilon_{m_j} \quad \text{in } \Omega^T_{m_j}. \tag{3}$$

The corresponding equation for the fracture is given by

$$\partial_t(\varepsilon^\kappa S_f(\psi^\varepsilon_f)) - \nabla \cdot \left(\varepsilon^\lambda K_f(S_f(\psi^\varepsilon_f))\nabla\psi^\varepsilon_f\right) = 0 \quad \text{in } \Omega^T_f. \tag{4}$$

We have used ε superscript to emphasise the dependence of the solution on this parameter. As already stated before, in the matrix $\psi^\varepsilon_{m_j}$ denotes the pressure head, S_m is the water saturation, K_m stands for the hydraulic conductivity, and f_{m_j} is a source or sink term. The water saturation S_m is a given function of $\psi^\varepsilon_{m_j}$, and the hydraulic conductivity is parametrised as a function of saturation, hence $K_m = K_m(S(\psi^\varepsilon_{m_j}))$. For simplicity, the gravity is here neglected, but all the results of this paper can be extended to include it. The analogous description is for the fracture equation.

In the above equations (3) and (4), we note the porosity and hydraulic conductivity scalings in the fracture with respect to that of the matrix. As suggested by the equations, we have assumed the following scaling for the porosity ϕ and the hydraulic conductivity in the fracture and the matrix blocks

$$\frac{\phi_f}{\phi_m} \propto \varepsilon^\kappa, \quad \text{and} \quad \frac{\bar{K}_{a,f}}{\bar{K}_{a,m}} \propto \varepsilon^\lambda, \tag{5}$$

where $\kappa, \lambda \in \mathbb{R}$ are scaling parameters; $\bar{K}_{a,f}$ and $\bar{K}_{a,m}$ denote the characteristic permeabilities in the fracture and the solid matrix, respectively. For the ease of notation, we take the constants of proportionality to be one for the analysis.

The transmission conditions on the matrix/fracture interface consist of the continuity of fluxes and that of pressure. The transmission condition for the normal component of the fluxes is

$$K_m(S_m(\psi^\varepsilon_{m_j}))\nabla\psi^\varepsilon_{m_j}\cdot\vec{n} = \varepsilon^\lambda K_f(S_f(\psi^\varepsilon_f))\nabla\psi^\varepsilon_f\cdot\vec{n} \qquad \text{on } \Gamma^T_j. \tag{6}$$

The continuity of pressure is given by,

$$\psi^\varepsilon_{m_j} = \psi^\varepsilon_f \qquad \text{on } \Gamma^T_j. \tag{7}$$

We will write down the above equations and transmission condition for flux in mixed form. Introducing $v^\varepsilon_{m_j}$ and v^ε_f as the Darcy flux in matrix blocks and fracture respectively, for each ε, the dimensionless model is given by

$$\text{Problem } \mathcal{P}_\varepsilon \begin{cases} \partial_t S_m(\psi^\varepsilon_{m_j}) + \nabla\cdot v^\varepsilon_{m_j} = f_{m_j} & \text{in } \Omega^T_{m_j},\\ v^\varepsilon_{m_j} = -K_m(S_m(\psi^\varepsilon_{m_j}))\nabla\psi^\varepsilon_{m_j} & \text{in } \Omega^T_{m_j},\\ \partial_t(\varepsilon^\kappa S_f(\psi^\varepsilon_f)) + \nabla\cdot v^\varepsilon_f = f^\varepsilon_f & \text{in } \Omega^T_f,\\ v^\varepsilon_f = -\varepsilon^\lambda K_f(S_f(\psi^\varepsilon_f))\nabla\psi^\varepsilon_f & \text{in } \Omega^T_f,\\ v^\varepsilon_{m_j}\cdot\vec{n} = v^\varepsilon_f\cdot\vec{n} & \text{on } \Gamma^T_j,\\ \psi^\varepsilon_{m_j} = \psi^\varepsilon_f & \text{on } \Gamma^T_j,\\ \psi^\varepsilon_\rho(0) = \psi_{\rho,I} & \text{in } \Omega_\rho. \end{cases}$$

In words, the model consists of Richards' equation in the fracture and the matrix blocks, supplemented with the continuity of flux and pressure as transmission conditions, and initial conditions. Problem $\mathcal{P}_\varepsilon$ must be complemented with boundary conditions on the outer boundary. For simplicity, we choose homogeneous Dirichlet boundary conditions.

Remark 1 (Non-dimensionalisation)**.** *The above dimensionless model has been obtained starting from a dimensional model and choosing reference quantities. Starting with a simple two-dimensional geometry consisting of two square solid matrix blocks with edge length L separated by a fracture of width l, we define* $\varepsilon := \frac{l}{L}$*, that is, the ratio of the fracture width to its length. We take L as the reference length scale. Since the pressure is continuous at the interfaces, we define a single reference pressure head for the entire domain,* $\bar{\psi} = L$*. For the matrix blocks and the fracture, we use different reference hydraulic conductivities* $\bar{K}_{a,m}$ *and* $\bar{K}_{a,f}$*, respectively. As the reference time scale, we set*

$$\bar{T} := \frac{\phi_m L^2}{\bar{K}_{a,m}\bar{\psi}} = \frac{\phi_m L}{\bar{K}_{a,m}}. \tag{8}$$

Treating the $\hat{}$ *superscripts as denoting the dimensional quantities, the dimensionless pressure heads are then given as* $\psi_{m_j} = \hat{\psi}_{m_j}/L$ *and* $\psi_f = \hat{\psi}_f/L$*, the dimensionless time as* $t = \hat{t}/\bar{T}$*, and the final time as* $T = \hat{T}/\bar{T}$*. As regards the source terms, we set* $f_{m_j} = \hat{f}_{m_j}\bar{T}/\phi_m$*. For more details, we refer to [36]*

Remark 2 (Scaling parameters)**.** *The scaling parameters* $\kappa, \lambda \in \mathbb{R}$ *are crucial in de-*

termining effective models in the limit $\varepsilon \to 0$. The value of κ determines the storage capacity of the fracture: for $\kappa < 0$, the reference porosity of the fracture increases for decreasing ε as compared to the reference porosity of the matrix blocks, and for $\kappa \leq -1$, the fracture maintains its ability to store water as ε approaches zero, as will be shown later. For $\kappa = 0$, no scaling occurs, and for $\kappa > 0$, the storage ability of the fracture decreases for $\varepsilon \to 0$ due to the decline of both the fracture volume (assuming fixed L) and the fracture porosity.

The parameter λ gives the scaling of the conductivities. $\lambda < 0$ corresponds to the case of a highly conductive fracture when compared to the matrix. This means that the flow through the fracture is more rapid. Whenever $\lambda > 0$ the fractures are less permeable than the blocks. The case $\lambda = 0$ means comparable conductivities. The case $\lambda \geq 1$ corresponds to impermeable fractures, leading in the limit $\varepsilon \to 0$ to models where the pressures at the matrix block at each side of the fractures are discontinuous.

3. Main result: Catalogue of effective models

Our main result is the derivation of effective models replacing the fracture by an interface. We provide the effective models for the range $(\kappa, \lambda) \in [-1, \infty) \times (-\infty, \infty)$.

3.1. Effective models

We subdivide the effective models into two major classes of models where the pressure head across the reduced dimensional fracture remains continuous as opposed to the effective models where the pressure head becomes discontinuous across the fracture. Among the first class, there are models in which the pressure becomes spatially constant.

3.1.1. Models with continuous pressure

Effective model I consists of the Richards equation in the matrix block subdomains and the one-dimensional Richards equation in the fracture. It occurs for $\kappa = \lambda = -1$.

Effective model I

$$
\begin{aligned}
\partial_t S_m(\psi_{m_j}) - \nabla \cdot \left(K_m(S_m(\psi_{m_j}))\nabla \psi_{m_j} \right) &= f_{m_j}, && \text{in } \Omega_{m_j}^T, \\
\partial_t S_f(\psi_f) - \partial_y \left(K_f(S_f(\psi_f))\partial_y \psi_f \right) &= [\vec{q}_m]_\Gamma, && \text{on } \Gamma^T, \\
\psi_{m_j} &= \psi_f, && \text{on } \Gamma^T, \\
\psi_{m_j}(0) &= \psi_{m_j,I}, && \text{on } \Omega_{m_j}, \\
\psi_f(0) &= \psi_{f,I}, && \text{on } \Gamma,
\end{aligned}
$$

where

$$
[\vec{q}_m]_\Gamma := \left(K_m(S_m(\psi_{m_1}))\nabla \psi_{m_1} \cdot \vec{n}_{m_1} + K_m(S_m(\psi_{m_2}))\nabla \psi_{m_2} \cdot \vec{n}_{m_2} \right) \Big|_\Gamma \tag{9}
$$

is the flux difference between the two solid matrix subdomains acting as a source term for Richards' equation in the fracture (note that $\vec{n}_{m_1} = -\vec{n}_{m_2}$). In this case the fracture has sufficient permeability to make the pressure therein x-independent. This also implies the continuity of the traces from the matrix side to the fracture pressure. Recall

that in the ε-scale model, there is continuity of flux. The jump in the flux on the right hand side in the fracture equation comes from the collapsing of the fracture subdomain to a one-dimensional object reflecting actually two interfaces.

Further, if the porosity ratio increases less than linearly with the reciprocal fracture width and the permeability ratio is taken to be reciprocally proportional to the fracture width, i.e. $\kappa > -1$ and $\lambda = -1$, one ends up with an effective model consisting of the Richards equation in the matrix blocks and a stationary elliptic equation in the fracture:

Effective model II

$$\begin{aligned}
\partial_t S_m(\psi_{m_j}) - \nabla \cdot \left(K_m(S_m(\psi_{m_j}))\nabla\psi_{m_j}\right) &= f_{m_j}, && \text{in } \Omega_{m_j}^T,\\
-\partial_y \left(K_f(S_f(\psi_f))\partial_y\psi_f\right) &= [\vec{q}_m]_\Gamma, && \text{on } \Gamma^T,\\
\psi_{m_j} &= \psi_f, && \text{on } \Gamma^T,\\
\psi_{m_j}(0) &= \psi_{m_j,I}, && \text{on } \Omega_{m_j}.
\end{aligned}$$

Note that, as before, there is again sufficient permeability in the fracture to ensure continuity of traces and the fracture pressure. Again, there is a jump of the flux on the right hand side of the fracture equation. The difference here from Effective model I is that the storage term vanishes in the limit because of κ being larger than -1.

On the other hand, only the flux term in the fracture vanishes in the limit for $\kappa = -1$ and $\lambda \in (-1, 1)$ reducing the model to an ordinary differential equation. This limit case corresponds to a fracture capable of storing and releasing water from the solid matrix, but which does not conduct fluid along the fracture. At the same time, continuity of traces of matrix pressure is retained, both equal to pressure in the fracture.

Effective model III

$$\begin{aligned}
\partial_t S_m(\psi_{m_j}) - \nabla \cdot \left(K_m(S_m(\psi_{m_j}))\nabla\psi_{m_j}\right) &= f_{m_j}, && \text{in } \Omega_{m_j}^T,\\
\partial_t S_f(\psi_f) &= [\vec{q}_m]_\Gamma, && \text{on } \Gamma^T,\\
\psi_{m_j} &= \psi_f, && \text{on } \Gamma^T,\\
\psi_{m_j}(0) &= \psi_{m_j,I}, && \text{on } \Omega_{m_j},\\
\psi_f(0) &= \psi_{f,I}, && \text{on } \Gamma.
\end{aligned}$$

Next, we consider the case when $\kappa > -1$ and $\lambda \in (-1, 1)$. As expected, both the storage term and the flow along the fracture have vanished. In this case, both the pressure and the flux are continuous on Γ. This behaves as if the fracture as a physical entity has disappeared.

Effective model IV

$$
\begin{aligned}
\partial_t S_m(\psi_{m_j}) - \nabla \cdot \left(K_m(S_m(\psi_{m_j}))\nabla\psi_{m_j}\right) &= f_{m_j}, && \text{in } \Omega_{m_j}^T,\\
[\vec{q}_m]_\Gamma &= 0, && \text{on } \Gamma^T,\\
\psi_{m_j} &= \psi_f, && \text{on } \Gamma^T,\\
\psi_{m_j}(0) &= \psi_{m_j,I}, && \text{on } \Omega_{m_j}.
\end{aligned}
$$

As we see from the preceding discussions, $\kappa = -1$ and $\lambda = 1$ are the critical cases. As long as $\lambda < 1$, there is continuity of the pressures at Γ (in the matrix) and the pressure in the fracture. Similarly, $\kappa > -1$ leads to the storage term dropping in the limit.

3.1.2. Models with discontinuous pressure

If the permeability ratio is proportional to the fracture width, i.e. $\lambda = 1$, the pressure in the effective models becomes discontinuous across the interface. For $\kappa = -1$, the pressure jump is determined by a parabolic differential equation on the spatial domain $(-\frac{1}{2}, \frac{1}{2})$, which does no longer represent a physical domain:

Effective model V

$$
\begin{aligned}
\partial_t S_m(\psi_{m_j}) - \nabla \cdot \left(K_m(S_m(\psi_{m_j}))\nabla\psi_{m_j}\right) &= f_{m_j}, && \text{in } \Omega_{m_j}^T,\\
\psi_{m_2} - \psi_{m_1} &= \left[\psi_f\right], && \text{on } \Gamma^T,\\
\psi_{m_j}(0) &= \psi_{m_j,I}, && \text{on } \Omega_{m_j},\\
\psi_f(0) &= \psi_{f,I}, && \text{for } z \in \left(-\frac{1}{2}, \frac{1}{2}\right), y \in \Gamma,
\end{aligned}
$$

where ψ_f solves for each y a parabolic differential equation in a one-dimensional domain:

$$
\begin{aligned}
\partial_t S_f(\psi_f) - \partial_z \left(K_f(S_f(\psi_f))\partial_z\psi_f\right) &= 0, && \text{for } z \in \left(-\frac{1}{2}, \frac{1}{2}\right), (t,y) \in \Gamma^T,\\
\psi_f(t, -\frac{1}{2}, y) &= \psi_{m_1}(t, 0, y), && \text{for } (t,y) \in \Gamma^T,\\
\left(K_f(S_f(\psi_f))\nabla\psi_f\right)(t, -\frac{1}{2}, y) \cdot \vec{n} &= \left(K_m(S_m(\psi_{m_1}))\nabla\psi_{m_1}\right)(t, 0, y) \cdot \vec{n}, && \text{for } (t,y) \in \Gamma^T,\\
\psi_f(t, \frac{1}{2}, y) &= \psi_{m_2}(t, 0, y), && \text{for } (t,y) \in \Gamma^T,\\
\left(K_f(S_f(\psi_f))\nabla\psi_f\right)(t, \frac{1}{2}, y) \cdot \vec{n} &= \left(K_m(S_m(\psi_{m_2}))\nabla\psi_{m_2}\right)(t, 0, y) \cdot \vec{n}, && \text{for } (t,y) \in \Gamma^T.
\end{aligned}
$$

Here

$$
\left[\psi_f\right] := \psi_f|_{z=\frac{1}{2}} - \psi_f|_{z=-\frac{1}{2}}. \tag{10}
$$

Similarly, in the effective model for $\kappa > -1$, the solution to a one-dimensional elliptic problem determines the pressure jump across the interface:

Effective model VI

$$\begin{aligned}
\partial_t S_m(\psi_{m_j}) - \nabla \cdot \left(K_m(S_m(\psi_{m_j}))\nabla\psi_{m_j}\right) &= f_{m_j}, && \text{in } \Omega^T_{m_j},\\
\psi_{m_2} - \psi_{m_1} &= \left[\psi_f\right], && \text{on } \Gamma^T,\\
\psi_{m_j}(0) &= \psi_{m_j,I}, && \text{on } \Omega_{m_j},
\end{aligned}$$

where ψ_f solves

$$\begin{aligned}
-\partial_z\left(K_f(S_f(\psi_f))\partial_z\psi_f\right) &= 0, && \text{for } z \in \left(-\frac{1}{2},\frac{1}{2}\right), (t,y) \in \Gamma^T,\\
\psi_f(t,-\frac{1}{2},y) &= \psi_{m_1}(t,0,y), && \text{for } (t,y) \in \Gamma^T,\\
\left(K_f(S_f(\psi_f))\nabla\psi_f\right)(t,-\frac{1}{2},y)\cdot\vec{n} &= \left(K_m(S_m(\psi_{m_1}))\nabla\psi_{m_1}\right)(t,0,y)\cdot\vec{n}, && \text{for } (t,y) \in \Gamma^T,\\
\psi_f(t,\frac{1}{2},y) &= \psi_{m_2}(t,0,y), && \text{for } (t,y) \in \Gamma^T,\\
\left(K_f(S_f(\psi_f))\nabla\psi_f\right)(t,\frac{1}{2},y)\cdot\vec{n} &= \left(K_m(S_m(\psi_{m_2}))\nabla\psi_{m_2}\right)(t,0,y)\cdot\vec{n}, && \text{for } (t,y) \in \Gamma^T.
\end{aligned}$$

If $\lambda > 1$, the permeability ratio decreases even faster as ε vanishes. Then we obtain effective models in which the pressure is discontinuous across the interface, and the subsolutions in the two solid matrix blocks and the fracture are entirely decoupled from each other, separated by a no-flow condition:

Effective model VII

$$\begin{aligned}
\partial_t S_m(\psi_{m_j}) - \nabla \cdot \left(K_m(S_m(\psi_{m_j}))\nabla\psi_{m_j}\right) &= f_{m_j}, && \text{in } \Omega^T_{m_j},\\
\partial_t S_f(\psi_f)(t,z,y) &= 0, && \text{for } z \in \left(-\frac{1}{2},\frac{1}{2}\right), (t,y) \in \Gamma^T,\\
K_m(S_m(\psi_{m_j}))\nabla\psi_{m_j}\cdot\vec{n}_{m_j} &= 0, && \text{on } \Gamma^T,\\
\psi_{m_j}(0) &= \psi_{m_j,I}, && \text{on } \Omega_{m_j},\\
\psi_f(0) &= \psi_{f,I}, && \text{for } z \in \left(-\frac{1}{2},\frac{1}{2}\right), y \in \Gamma.
\end{aligned}$$

In the above model, which corresponds to $\kappa = -1$, the physical quantities are assigned to the fracture, whereas the fracture is merely a geometrical entity that blocks the flow

in the effective model for $\kappa > -1$:

Effective model VII*

$$\begin{aligned}
\partial_t S_m(\psi_{m_j}) - \nabla \cdot \left(K_m(S_m(\psi_{m_j}))\nabla\psi_{m_j}\right) &= f_{m_j}, && \text{in } \Omega_{m_j}^T,\\
K_m(S_m(\psi_{m_j}))\nabla\psi_{m_j} \cdot \vec{n}_{m_j} &= 0, && \text{on } \Gamma^T,\\
\psi_{m_j}(0) &= \psi_{m_j,I}, && \text{on } \Omega_{m_j}.
\end{aligned}$$

3.1.3. Models with spatially constant pressure in the fracture

A subclass of models with continuous pressure at the interface is obtained when the permeability in the fracture becomes so large that any pressure fluctuation is instantaneously equalised, that is, the pressure within the fracture becomes constant in the limit of vanishing fracture width. Note that this cannot occur if the fracture boundary conditions are incompatible with a spatially constant pressure as in the case of Dirichlet boundary conditions that fix different pressures at the fracture endpoints.
In the case $\kappa = -1$ and $\lambda < -1$, one gets:

Effective model VIII

$$\begin{aligned}
\partial_t S_m(\psi_{m_j}) - \nabla \cdot \left(K_m(S_m(\psi_{m_j}))\nabla\psi_{m_j}\right) &= f_{m_j}, && \text{in } \Omega_{m_j}^T,\\
\psi_f(t,y) &= \psi_f(t), && \text{on } \Gamma^T,\\
\partial_t S_f(\psi_f)(t) &= \int_0^1 [\vec{q}_m]_\Gamma \, dy, && \text{on } \Gamma^T,\\
\psi_{m_j} &= \psi_f, && \text{on } \Gamma^T,\\
\psi_{m_j}(0) &= \psi_{m_j,I}, && \text{on } \Omega_{m_j},\\
\psi_f(0) &= \psi_{f,I}, && \text{on } \Gamma.
\end{aligned}$$

Since the pressure is spatially constant and continuous in the fracture, the pressure in the solid matrices at the interface must be spatially constant as well. The ordinary differential equation for the saturation in the fracture expresses the storage of inflowing water in the fracture.
For $\kappa > -1$ and $\lambda < -1$, the storage term in the fracture vanishes and the pressure in the fracture takes a constant value at each point in time. This value is determined in such a way that the total flux across the fracture is conserved:

Effective model IX

$$\begin{aligned}
\partial_t S_m(\psi_{m_j}) - \nabla \cdot \left(K_m(S_m(\psi_{m_j}))\nabla\psi_{m_j}\right) &= f_{m_j}, && \text{in } \Omega_{m_j}^T,\\
\psi_f(t,y) &= \psi_f(t), && \text{on } \Gamma^T,\\
\int_0^1 [\vec{q}_m]_\Gamma \, dy &= 0, && \text{on } \Gamma^T,\\
\psi_{m_j} &= \psi_f, && \text{on } \Gamma^T,\\
\psi_{m_j}(0) &= \psi_{m_j,I}, && \text{on } \Omega_{m_j}.
\end{aligned}$$

Remark 3. *We comment on Effective models V and VI above. Note that the solution in the fracture depends on z. Also, $z = -\frac{1}{2}$ corresponds to the porous matrix domain Ω_{m_1} having the interface at $x = 0$. Similarly, Ω_{m_2} has the interface at $x = 0$ with the fracture domain boundary at $z = \frac{1}{2}$. This is a "two-scale" type of model where the permeability has the scaling such that the collapsing of the fracture interface is not justified. Similar models, in the context of reactive flow, are derived in [41]. This is in contrast to the Effective models I–IV where the solution in the fracture domain is independent of z and the fracture collapses as an interface. Also the two interfaces from the porous matrix sides coincide.*

3.2. Comparison with existing models

We make a brief comparison with the fracture models that are widely used in practice (see e.g., [9, 25, 51]). We refer to [37] where similar models are derived for single phase flow, but the interface conditions are relevant to us (see for example [3] for the extension to two-phase flow models). The comparison is in two respects: in terms of derivation of the effective model, and secondly in terms of the final results obtained.

The derivation in [37] takes place in three steps. First, the Darcy flow equation along the fracture surface is obtained immediately by considering the flux component in the tangential direction of the fracture. Second, one integrates the flow equation along the transverse direction in the fracture subdomain. Using the continuity of fluxes at the matrix/fracture interfaces, this yields a surface equation with the jump in the matrix flux term as a source term. Note that the second step yields a fracture equation in the integral form on the left hand side. The third step is a closure relationship by *postulating* a pressure profile in the fracture. This is in contrast with our approach. We assume a scaling of hydraulic properties on ε and use a formal asymptotic ansatz. But once the choice of scaling is made, the rest of the steps follow without any additional assumptions. In particular, our approach does not postulate any closure condition on the pressure inside the fracture as this is part of the solution. Having an assumed scaling of fracture permeability on the width *allows deducing* the pressure profile inside the fracture. Also we mention that in [37], the closure condition introduces a parameter in the effective model for the fracture. Here, we have a catalogue of models and no additional parameter is necessary. Moreover, for several of the regimes considered here, the derivation is sustained by mathematically rigorous proofs (see [36]).

The interface conditions as derived in [37] (Eqns. (3.18), (3.19) on pp. 1672) read *mutatis mutandis*,

$$
\begin{aligned}
-\xi v_{m_1} \cdot n_1|_{\Gamma_1} + \alpha_f \psi_{m_1}|_{\Gamma_1} &= -(1-\xi) v_{m_2} \cdot n_2|_{\Gamma_2} + \alpha_f \psi_f, \\
-\xi v_{m_2} \cdot n_2|_{\Gamma_1} + \alpha_f \psi_{m_2}|_{\Gamma_2} &= -(1-\xi) v_{m_1} \cdot n_1|_{\Gamma_1} + \alpha_f \psi_f,
\end{aligned}
$$

where we once again emphasise that the above results are derived for a single phase steady state flow model. Here, $\alpha_f := \bar{K}_{a,f}/\varepsilon = \varepsilon^{\lambda-1}\bar{K}_{a,m}$ and ξ is a parameter introduced during closure conditions. In terms of ε and rearranging terms we have (modulo a

constant factor),

$$\varepsilon^{\lambda-1}\left(\psi_{m_1}|_{\Gamma_1}-\psi_f\right)=-(1-\xi)v_{m_2}\cdot n_2|_{\Gamma_2}+\xi v_{m_1}\cdot n_1|_{\Gamma_1},$$
$$\varepsilon^{\lambda-1}\left(\psi_{m_2}|_{\Gamma_2}-\psi_f\right)=-(1-\xi)v_{m_1}\cdot n_1|_{\Gamma_1}+\xi v_{m_2}\cdot n_2|_{\Gamma_2}.$$

Now, for $\lambda > 1$, and for the choice of $\xi = 1$, we immediately see that we get a no-flow boundary condition (compare with the Effective models VII and VII* here). On the other hand, for any value of ξ, for $\lambda < 1$, as ε goes to zero, we get $\psi_1 = \psi_f$ on Γ_1 and $\psi_2 = \psi_f$ on Γ_2 and Γ_1, Γ_2 collapse on the same surface (compare with Effective models I–IV). When $\lambda = 1$, by postulating a profile inside the fracture (e.g., linear) the above interface conditions provide an effective equation. Here, this postulate is replaced by a differential equation inside the fracture to resolve the pressure profile therein.

4. Formal upscaling and derivation of effective models

We perform a formal upscaling for the above system of equations to derive the effective equations. For the quantities in the subdomain Ω_ρ, ($\rho \in \{m_1, m_2, f\}$), one makes the following ansatz:

$$\begin{array}{lcllll}
\psi^\varepsilon_{m_1} & = & \psi^0_{m_1} & + & \varepsilon\psi^1_{m_1} & + & O(\varepsilon^2),\\
\psi^\varepsilon_{m_2} & = & \psi^0_{m_2} & + & \varepsilon\psi^1_{m_2} & + & O(\varepsilon^2),\\
\psi^\varepsilon_{f} & = & \psi^0_{f} & + & \varepsilon\psi^1_{f} & + & O(\varepsilon^2),\\
v^\varepsilon_{m_1} & = & v^0_{m_1} & + & \varepsilon v^1_{m_1} & + & O(\varepsilon^2),\\
v^\varepsilon_{m_2} & = & v^0_{m_2} & + & \varepsilon v^1_{m_2} & + & O(\varepsilon^2).
\end{array}$$

4.1. The models in matrix blocks Ω_{m_j}

We treat the case for $j = 1$; $j = 2$ is identical. Inserting the expansion for $\psi^\varepsilon_{m_1}$ in the model equation, we obtain up to an approximation of $O(\varepsilon^2)$

$$\begin{aligned}
\partial_t(S_m(\psi^0_{m_1}+\varepsilon\psi^1_{m_1})+\nabla\cdot(v^0_{m_1}+\varepsilon v^1_{m_1}) &= f_{m_1} && \text{in } \Omega^T_{m_1},\\
v^0_{m_1}+\varepsilon v^1_{m_1} &= -K_m(S_m(\psi^0_{m_1}+\varepsilon\psi^1_{m_1}))(\nabla\psi^0_{m_1}+\varepsilon\psi^1_{m_1}) && \text{in } \Omega^T_{m_1}.
\end{aligned}$$

Equating the respective orders of ε, we obtain up to the leading order (that is up to $O(\varepsilon)$),

$$\begin{aligned}
\partial_t(S_m(\psi^0_{m_1}))+\nabla\cdot v^0_{m_1} &= f_{m_1} && \text{in } \Omega^T_{m_1},\\
v^0_{m_1} &= -K_m(S_m(\psi^0_{m_1}))\nabla\psi^0_{m_1} && \text{in } \Omega^T_{m_1}.
\end{aligned}$$

For $j = 2$, the equation is identical:

$$\begin{aligned}
\partial_t(S_m(\psi^0_{m_2})+\nabla\cdot v^0_{m_2} &= f_{m_2} && \text{in } \Omega^T_{m_2},\\
v^0_{m_2} &= -K_m(S_m(\psi^0_{m_2}))\nabla\psi^0_{m_2} && \text{in } \Omega^T_{m_2}.
\end{aligned}$$

Note that this is expected that in the subdomain we retain the same equation.

4.2. The model in the fracture subdomain Ω_f

To treat the fracture equation, first we map the domain Ω_f to an ε independent domain. The coordinate transformation $(x, y) \mapsto (z = x/\varepsilon, y)$ transforms the domain Ω_f to a fixed domain $\tilde{\Omega}_f := (-\frac{1}{2}, \frac{1}{2}) \times (0, 1)$. In terms of (z, y) coordinates, the transformed equation reads

$$\begin{aligned} \partial_t(\varepsilon^\kappa S_f(\psi_f^\varepsilon)) + (\frac{1}{\varepsilon}\partial_z\psi_f^\varepsilon, \partial_y\psi_f^\varepsilon)^T \cdot v_f^\varepsilon = 0 \qquad & \text{in } \tilde{\Omega}_f^T, \\ v_f^\varepsilon = -\varepsilon^\lambda K_f(S_f(\psi_f^\varepsilon))(\frac{1}{\varepsilon}\partial_z\psi_f^\varepsilon, \partial_y\psi_f^\varepsilon)^T \qquad & \text{in } \tilde{\Omega}_f^T. \end{aligned}$$

We put the two equations together, eliminating v_f^ε, we have,

$$\partial_t(\varepsilon^\kappa S_f(\psi_f^\varepsilon)) - \varepsilon^\lambda \left(\partial_y(K_f(S_f(\psi_f^\varepsilon))\partial_y\psi_f^\varepsilon) + \frac{1}{\varepsilon^2}\partial_z(K_f(S_f(\psi_f^\varepsilon))\partial_z\psi_f^\varepsilon) \right) = 0 \qquad \text{in } \tilde{\Omega}_f^T.$$

Inserting the expansion for ψ_f^ε and restricting to the leading order term, we obtain, up to the accuracy of $O(\varepsilon)$

$$\partial_t(\varepsilon^\kappa S_f(\psi_f^0)) - \varepsilon^\lambda \left(\partial_y(K_f(S_f(\psi_f^0))\partial_y\psi_f^0) + \frac{1}{\varepsilon^2}\partial_z(K_f(S_f(\psi_f^0))\partial_z\psi_f^0) \right) = 0 \qquad \text{in } \tilde{\Omega}_f^T. \tag{11}$$

4.3. The transmission conditions at Γ_j

Writing the transmission conditions in the (x, z) co-ordinates, and expanding in powers of ε, up to $O(\varepsilon^2)$

$$\psi_{m_j}^0 + \varepsilon\psi_{m_j}^1 = \psi_f^0 + \varepsilon\psi_f^1 \qquad \text{at } \Gamma_j^T.$$

Equating the respective powers of ε, and noting the co-ordinate transformation for the fracture subdomain,

$$\begin{aligned} \psi_{m_1}^0(x = 0) = \psi_f^0(z = -\frac{1}{2}), \quad \psi_{m_2}^0(x = 0) = \psi_f^0(z = \frac{1}{2}), \\ \psi_{m_1}^1(x = 0) = \psi_f^1(z = -\frac{1}{2}), \quad \psi_{m_2}^1(x = 0) = \psi_f^1(z = \frac{1}{2}). \end{aligned} \tag{12}$$

Next, we treat the flux term. Inserting the expansion and retaining only the leading order term, we obtain

$$\begin{aligned} -K_m(S_m(\psi_{m_1}^0))\partial_x\psi_{m_1}^0(x = 0) = -\varepsilon^{\lambda-1}K_f(S_f(\psi^0))\partial_z\psi_f^0(z = -\frac{1}{2}) \\ -K_m(S_m(\psi_{m_2}^0))\partial_x\psi_{m_2}^0(x = 0) = -\varepsilon^{\lambda-1}K_f(S_f(\psi^0))\partial_z\psi_f^0(z = \frac{1}{2}). \end{aligned} \tag{13}$$

We conclude, for $\lambda > 1$

$$-K_m(S_m(\psi_{m_j}^0))\partial_x\psi_{m_j}^0 = 0 \qquad \text{on } \Gamma^T. \tag{14}$$

For $\lambda = 1$, we have

$$-K_m(S_m(\psi^0_{m_1}))\partial_x\psi^0_{m_1}(x=0) = -K_f(S_f(\psi^0))\partial_z\psi^0_f(z=-\frac{1}{2}),$$
$$-K_m(S_m(\psi^0_{m_2}))\partial_x\psi^0_{m_2}(x=0) = -K_f(S_f(\psi^0))\partial_z\psi^0_f(z=\frac{1}{2}).$$

4.4. Derivation of the models

For $\kappa = -1, \lambda = -1$, taking the lower order of ε in (11) gives

$$\partial_z(K_f(S_f(\psi^0_f))\partial_z\psi^0_f) = 0 \qquad \text{in } \hat{\Omega}^T_f,$$

which implies,

$$K_f(S_f(\psi^0_f))\partial_z\psi^0_f = C.$$

Now use the interface condition (13) to conclude that, up to order $O(\varepsilon)$, $K_f(S_f(\psi^0_f))\partial_z\psi^0_f = 0$. Here we have assumed that $-K_m(S_m(\psi^0_{m_j}))\partial_x\psi^0_{m_j}$ is an $O(1)$ quantity. Now using the non-degeneracy of K_f, we conclude $\partial_z\psi^0_f = 0$, making ψ^0_f independent of z. We further integrate (11) over $z = -\frac{1}{2}$ to $\frac{1}{2}$ to get,

$$\int_{-1/2}^{1/2}\left(\partial_t(S_f(\psi^0_f)) - \partial_y(K_f(S_f(\psi^0_f))\partial_y\psi^0_f)\right)dz = \varepsilon^{-2}\left((K_f(S_f(\psi^0_f))\partial_z\psi^0_f)_{z=\frac{1}{2}} - (K_f(S_f(\psi^0_f))\partial_z\psi^0_f)_{z=-\frac{1}{2}}\right)$$
$$= [\vec{q}_m]_\Gamma,$$

where

$$[\vec{q}_m]_\Gamma := \left(K_m(S_m(\psi^0_{m_1}))\nabla\psi^0_{m_1}\cdot\vec{n}_{m_1} + K_m(S_m(\psi^0_{m_2}))\nabla\psi^0_{m_2}\cdot\vec{n}_{m_2}\right)\Big|_\Gamma$$
$$= \left(K_m(S_m(\psi^0_{m_2}))\partial_x\psi^0_{m_2} - K_m(S_m(\psi^0_{m_1}))\partial_x\psi^0_{m_1}\right)\Big|_\Gamma,$$

and we have used the continuity of flux interface condition (13). Finally, using the z-independence of ψ^0_f, we get the equation in the reduced dimension fracture,

$$\partial_t S_f(\psi^0_f) - \partial_y\left(K_f(S_f(\psi^0_f))\partial_y\psi^0_f\right) = [\vec{q}_m]_\Gamma, \qquad \text{on } \Gamma^T. \tag{15}$$

Together with (12), and with the boundary conditions and initial conditions inherited from the original ε model, we get the model termed as Effective model I.

Next, we consider the case when $\kappa \in (-1, \infty)$, $\lambda = -1$. The only thing that changes in the above derivation is the storage term. Instead of repeating all the steps, we just write down the main steps. As before, we obtain

$$\int_{-1/2}^{1/2}\left(\varepsilon^{\kappa+1}\partial_t(S_f(\psi^0_f)) - \partial_y(K_f(S_f(\psi^0_f))\partial_y\psi^0_f)\right)dz = [\vec{q}_m]_\Gamma.$$

We have used again the continuity of flux at the matrix/fracture interface (13). Finally, using the z-independence of ψ^0_f, and noting that the first term on the left side drops as

ε vanishes, we get the equation on the fracture surface,

$$-\partial_y \left(K_f(S_f(\psi_f^0))\partial_y \psi_f^0 \right) = [\vec{q}_m]_\Gamma \qquad \text{on } \Gamma^T. \tag{16}$$

Together with (12) and the boundary conditions and initial conditions inherited from the original ε model, we get the model termed as Effective model II.

For $\kappa = -1, \lambda \in (-1, 1)$, as before using (13) we obtain $K_f(S_f(\psi_f^0))\partial_z \psi_f^0 = 0$. Integrating (11) over $(-\frac{1}{2}, \frac{1}{2})$ gives

$$\int_{-1/2}^{1/2} \left(\partial_t (S_f(\psi_f^0)) - \varepsilon^{\lambda+1} \partial_y (K_f(S_f(\psi_f^0))\partial_y \psi_f^0) \right) dz = [\vec{q}_m]_\Gamma ,$$

and as above we have used the continuity of flux at the matrix/fracture interface (13). Finally, using the z-independence of ψ_f^0, and noting that the second term on the left side drops as ε vanishes, we get the equation on the fracture surface,

$$\partial_t S_f(\psi_f^0) = [\vec{q}_m]_\Gamma \qquad \text{on } \Gamma^T. \tag{17}$$

Together with (12), the boundary conditions and initial conditions inherited from the original ε model give Effective model III.

The Effective model IV corresponds to $\kappa \in (-1, \infty)$, $\lambda \in (-1, 1)$. The arguments are already covered. For $\lambda \in (-1, 1)$, we use (13) to obtain $K_f(S_f(\psi_f^0))\partial_z \psi_f^0) = 0$, implying the z-independence of ψ_f^0. Again, integrating (11) over $(-\frac{1}{2}, \frac{1}{2})$ gives

$$\int_{-1/2}^{1/2} \left(\varepsilon^{\kappa+1} \partial_t (S_f(\psi_f^0)) - \varepsilon^{\lambda+1} \partial_y (K_f(S_f(\psi_f^0))\partial_y \psi_f^0) \right) dz = [\vec{q}_m]_\Gamma .$$

As above we have used the continuity of flux at the matrix/fracture interface (13). Finally, using the z-independence of ψ_f^0, and noting that both the first term and the second term on the left side drop as ε vanishes, we get the equation in the upscaled fracture

$$[\vec{q}_m]_\Gamma = 0.$$

The other equations are as expected yielding Effective model IV.

Next we treat the case $\kappa = -1, \lambda = 1$. For $\lambda = 1$, we have the interface condition,

$$\begin{aligned} -K_m(S_m(\psi_{m_1}^0))\partial_y \psi_{m_1}^0(x = 0) &= -K_f(S_f(\psi^0))\partial_z \psi_f^0(z = -\frac{1}{2}), \\ -K_m(S_m(\psi_{m_2}^0))\partial_y \psi_{m_2}^0(x = 0) &= -K_f(S_f(\psi^0))\partial_z \psi_f^0(z = \frac{1}{2}), \end{aligned} \tag{18}$$

giving the flux and the continuity of the pressure

$$\psi^0_{m_1}(y=0) = \psi^0_f(z=-\frac{1}{2}), \quad \psi^0_{m_2}(y=0) = \psi^0_f(z=\frac{1}{2}). \tag{19}$$

In this case, we do not have the flux inside the fracture vanishing as ε goes to zero. This means that ψ^0_f may not be independent of z. Thus, the usual process of integrating as done in the previous models does not help. On the other hand, the simple co-ordinate transformation that we have already done for the fracture subdomain already helps in getting the effective model. The equation in the fracture subdomain reads,

$$\varepsilon^{-1}\partial_t(S_f(\psi^0_f)) - \varepsilon\partial_y(K_f(S_f(\psi^0_f))\partial_y\psi^0_f) - \varepsilon^{-1}\partial_z\left((K_f(S_f(\psi^0_f))\partial_z\psi^0_f)\right) = 0.$$

This in the limit provides the fracture equation,

$$\partial_t(S_f(\psi^0_f)) - \partial_z\left((K_f(S_f(\psi^0_f))\partial_z\psi^0_f)\right) = 0 \quad \text{for } z \in \left(-\frac{1}{2},\frac{1}{2}\right), (t,y) \in \Gamma^T.$$

The interface conditions (18) and (19) and the subdomain equation complete the model derivation.

Next we treat the case $\kappa = (-1,\infty), \lambda = 1$. This is the same as the previous model except for the scaling of κ in the storage term. The interface conditions (18) and (19) remain the same as in Model V. Again ψ^0_f may be dependent on z. Accordingly, the equation in the fracture subdomain reads

$$\varepsilon^{\kappa+1}\partial_t(S_f(\psi^0_f)) - \varepsilon^2\partial_y(K_f(S_f(\psi^0_f))\partial_y\psi^0_f) - \partial_z\left((K_f(S_f(\psi^0_f))\partial_z\psi^0_f)\right) = 0$$

and in the limit it provides the fracture equation with the first and second term dropping out,

$$-\partial_z\left((K_f(S_f(\psi^0_f))\partial_z\psi^0_f)\right) = 0 \text{ for } z \in \left(-\frac{1}{2},\frac{1}{2}\right), (t,y) \in \Gamma^T.$$

Together with the interface conditions (18) and (19) and retaining the subdomain equation, this complete the derivation of Effective model VI. The dependency of ψ^0_f on t and y happens via the interface conditions. Recall Remark 3 where we commented that in the above models (namely V and VI), the fracture model does not collapse in a reduced dimensional fracture models and one needs to solve a differential equation inside the fracture subdomain (and not on the surface as done in the Effective models I – IV). This is a "two-scale" type effect, similar to a cell problem in homogenisation.

In the next two models, the permeability in the fracture is sufficiently low so that the fracture acts as a barrier. We will jointly treat the cases when $\kappa = -1, \lambda \in (1,\infty)$ and $\kappa \in (-1,\infty), \lambda \in (1,\infty)$. The difference between the two cases is the scaling of the storage term and as we have seen before, the storage term will not survive in the latter case. Both of these cases are straightforward. The subdomain equations remains unchanged as before. We then recall the interface condition (14) to deduce the

boundary condition for the matrix subdomain,

$$K_m(S_m(\psi^0_{m_j}))\nabla\psi^0_{m_j}\cdot\vec{n}_{m_j} = 0, \qquad \text{on } \Gamma^T.$$

This is the no-flow boundary condition for the matrix subdomain equation at the fracture/subdomain interface and can be solved independently. Thus, the fracture equation becomes irrelevant. However, for $\kappa = -1$, we can still evaluate the fracture equation by solving the differential equation,

$$\partial_t S_f(\psi^0_f)(t,z,y) = 0, \qquad \text{for } z \in \left(-\frac{1}{2},\frac{1}{2}\right), (t,y) \in \Gamma^T,$$

as the flux terms in the fracture drop out. In the case when $\kappa \in (-1,\infty)$, $\lambda \in (1,\infty)$, even the storage term drops out making the fracture irrelevant. Together with retaining the initial condition and the boundary conditions, we recover Effective model VII and VII*.

Finally we comment on the effective equations VIII and IX. These correspond to $\kappa = -1, \lambda \in (-\infty,-1)$ and $\kappa \in (-1,\infty), \lambda \in (-\infty,-1)$, respectively. Note that in both cases, the fracture permeability is large enough to yield independence of pressure with respect to the z co-ordinate. In addition, the fracture pressure also becomes independent of the y co-ordinate. In case $\kappa = -1$, the storage term survives and the fracture pressure only depends on t. This provides Effective model VIII. Effective model IX results when the storage term also drops out. We spare the details as they are analogous to the arguments already discussed before.

4.5. Summary of the effective models

For the readers' convenience, we summarise the effective model according to the range of parameters κ and λ.

$$\begin{aligned}
&\kappa = -1, && \lambda = -1 : && \text{Effective model I},\\
&\kappa \in (-1,\infty), && \lambda = -1 : && \text{Effective model II},\\
&\kappa = -1, && \lambda \in (-1,1) : && \text{Effective model III},\\
&\kappa \in (-1,\infty), && \lambda \in (-1,1) : && \text{Effective model IV},\\
&\kappa = -1, && \lambda = 1 : && \text{Effective model V},\\
&\kappa \in (-1,\infty), && \lambda = 1 : && \text{Effective model VI},\\
&\kappa = -1, && \lambda \in (1,\infty) : && \text{Effective model VII},\\
&\kappa \in (-1,\infty), && \lambda \in (1,\infty) : && \text{Effective model VII}^*,\\
&\kappa = -1, && \lambda \in (-\infty,-1) : && \text{Effective model VIII},\\
&\kappa \in (-1,\infty), && \lambda \in (-\infty,-1) : && \text{Effective model IX}.
\end{aligned} \tag{20}$$

5. Numerical examples

The aim of this section is to validate the results of the theoretical upscaling numerically. For all simulations, we use a simple finite volume scheme on a static, uniform

grid with rectangular cells, implemented in MATLAB. Fluxes are computed with a two-point flux approximation scheme. An implicit Euler method with fixed time step is used for the time discretisation and we employ a modified Picard scheme for the linearisation procedure. For simplicity, the problem is solved monolithically in the entire coupled domain instead of harnessing a domain decomposition scheme.

In our numerical example, we consider a realistic, dimensional setting in order to investigate how well the effective models approximate the full model for different soil properties. The example is inspired by [52] and deals with the filling of a reservoir that is crossed by a horizontal fracture. Since we assume the geometry to be symmetric, it is sufficient to simulate one half of the geometry (see Figure 2). The filling of the reservoir is modelled by a time-dependent Dirichlet condition at the upper domain boundary and we impose no-flow conditions everywhere at the outer boundary except in the lower right corner, where the pressure head is kept fixed. This means that in order for the injected water to leave the domain, it must travel through the fracture, which can either hinder or facilitate the flow, depending on the fracture's hydraulic properties.

To be specific, we define the geometry as $\Omega_{m_1} = (0,2) \times (0,l)$, $\Omega_{m_2} = (0,2) \times (1.1, 2.2)$, $\Omega_f = (0,2) \times (1.1 - l, 1.1)$, where the parameter l determines the fracture width. Initially, the entire domain is in a hydrostatic equilibrium state given by

$$\psi_I(x,z) = -0.5 - z. \tag{21}$$

We subdivide the domain boundary into $\partial\Omega = \Gamma_{D_1} \cup \Gamma_{D_2} \cup \Gamma_N$, where $\Gamma_{D_1} = \{2\} \times (0, 0.5)$, $\Gamma_{D_2} = (0,1) \times \{2.2\}$, and $\Gamma_N = \partial\Omega \setminus (\Gamma_{D_1} \cup \Gamma_{D_2})$ is the remaining boundary, and impose the boundary conditions

$$\psi(t,x,z) = \begin{cases} -0.5 - z, & \text{on } \Gamma_{D_1}, \\ -1.6 + 0.6\,t, & \text{for } t < 3 \text{ on } \Gamma_{D_2}, \\ 0.2, & \text{for } t \geq 3 \text{ on } \Gamma_{D_2}, \end{cases} \tag{22}$$

and

$$\nabla\psi(t,x,z) \cdot \vec{n} = 0, \text{ on } \Gamma_N, \tag{23}$$

where $\vec{n}$ denotes the normal vector on the outer domain boundary.

In this example, we denote the horizontal co-ordinate with x and the vertical co-ordinate with z such that gravity points in negative z-direction as usual. Note that this contrasts with the use of x and z in the theoretical part. The spatial grid consists of square cells with $\Delta x = \Delta y = 1$ *cm* in the solid matrix blocks as well as for fractures of $10 - 20$ *cm* width; for fractures of 1 *cm* width, we choose $\Delta x = 1$ *cm* and $\Delta z = 0.1$ *cm* in order to resolve the fracture appropriately. The fracture equation in the effective models is discretised on a one-dimensional grid with $\Delta x = 1$ *cm*.

Although not presented in the theoretical part of this work, gravity is included in these simulations in order to make the problem setup more interesting – the extension of the theoretical upscaling to include gravity is immediate.
The soil parameters that we consider are taken from [22] and [32] and listed in Table 1.

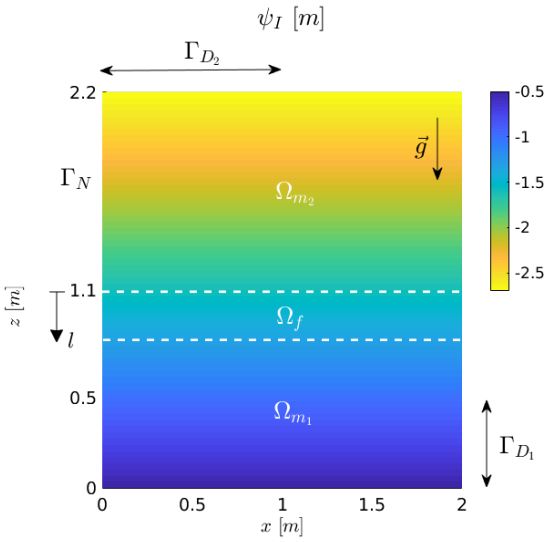

Figure 2: Scheme of the geometry with boundary and initial conditions for the realistic example

Since the simulation uses dimensional quantities, the flux and storage term are not scaled with powers of ε. Let us emphasise that the hydraulic quantities do not change depending on different fracture widths that we consider. Although smaller fracture widths lead to a slightly larger lower solid matrix block since we keep the size of the coupled simulation domain fixed, we expect this effect to be small compared to the impact of the smaller fracture width itself on the fluid flow.

Name	Guelph loam	Hygiene sandstone	Silt loam	Touchet silt loam	UNSODA 4030
α $[m^{-1}]$	1.15	0.79	0.423	0.50	4.32
θ_S $[-]$	0.520	0.250	0.396	0.469	0.415
θ_R $[-]$	0.218	0.153	0.131	0.190	0.0
n_{VG} $[-]$	2.76	10.4	2.06	7.09	1.41
K_S $[m\,d^{-1}]$	0.316	1.08	0.0496	3.03	0.0116

Table 1: Van Genuchten parameters of the soils for the realistic example

5.1. Soils with similar properties

First, let us investigate the case of two soils with similar permeability and porosity (note that the van Genuchten parameter θ_S corresponds to porosity if we assume that the entire pore space is accessible to the water), i.e. the regime $\kappa, \lambda \approx 0$.

We choose the simulation end time to be $T = 4\ d$ and the time step is taken to be $\Delta t = 0.05\ d$. We consider two fracture widths, $l = 10\ cm$ and $l = 1\ cm$, and compare the solution of the full models to the solution of the corresponding effective model.

The solid matrices are taken to be composed of drying Guelph loam, while the fracture is made up of Hygiene sandstone. Thus, the ratio between the permeabilities and porosities is well within one order of magnitude and we expect the solution to converge towards Effective model IV, where the flow is continuous across the fracture and the storage and the flux terms in the fracture have vanished.

In detail, this can be seen by plugging in the soil properties into equation (5) and using $\varepsilon = l/L$, which gives $\kappa \approx 0.24, 0.14$ and $\lambda \approx -0.41, -0.23$ for $l = 10\ cm, 1\ cm$, respectively. This means that $\kappa > -1$ and $\lambda \in (-1, 1)$ for both fracture widths under consideration, corresponding to the parameter range of Effective model IV. Since we do explicitly not scale the soil parameters with the fracture width in the spirit of a convergence study but rather investigate how well the limit models approximate realistic scenarios, the absolute value of the scaling parameters becomes smaller for smaller fracture widths due to the fixed left hand side in equation (5).

Figure 3 shows the solution in intervals of a day (from top to bottom) for the case of a 10 cm thick fracture. As the simulation starts in hydrostatic equilibrium, the hydraulic head is initially constant; then, it increases over time beginning from the upper left corner where the reservoir is being filled. Note that whereas the pressure head is continuous at the fracture because of the pressure interface condition, the saturation is discontinuous since the parametrisations of the saturation in the fracture and the solid matrix differ from each other. It is clearly visible that the flow in the fracture is slightly faster than in the surrounding matrix blocks due to the slightly higher permeability: after three days, the water in the fracture has already reached the right domain boundary (see the hydraulic head in Figure 3) as opposed to the matrix blocks where the right domain boundary is still dry. After four days, almost the entire domain is saturated except for the area around Γ_{D_1} where the pressure is kept fixed, and the upper right corner that the flow has not reached yet.

The z-averaged pressure head at final time is plotted in Figure 4. As expected, Effective model IV gives an excellent approximation of the full model in case of a thin fracture and it is apparent that the fracture solution of the full model converges towards the effective model as the fracture width goes to zero. For larger fracture widths, the slightly higher permeability of the fracture as compared to the solid matrix blocks means that the fracture is the preferred flow path and water is discharged along the fracture, leading to a higher pressure on the right hand side as compared to the effective model. As the fracture width becomes smaller, the fracture gradually loses its ability to store water and to transport water along the fracture owing to its decreasing volume, culminating in Effective model IV where the fracture as a physical object has disappeared.

We also show the result for Effective model III, where the storage term remains and the flux term has vanished. This effective model gives a lower pressure than the full models, which is a consequence of the fracture's ability to store water.

Note that simply approximating a thin fracture by the one-dimensional Richards equation (Effective model I) leads to a massive overestimation of the fracture's ability to store water and to conduct flow. This can also be seen in Figure 5, where the cumulative outflow across the lower right Dirichlet boundary over time is depicted in a logarithmic scale. Notice that the unit m^2/d reflects the fact that our geometry is two-dimensional. During the first two days, the inflow has not yet reached the lower

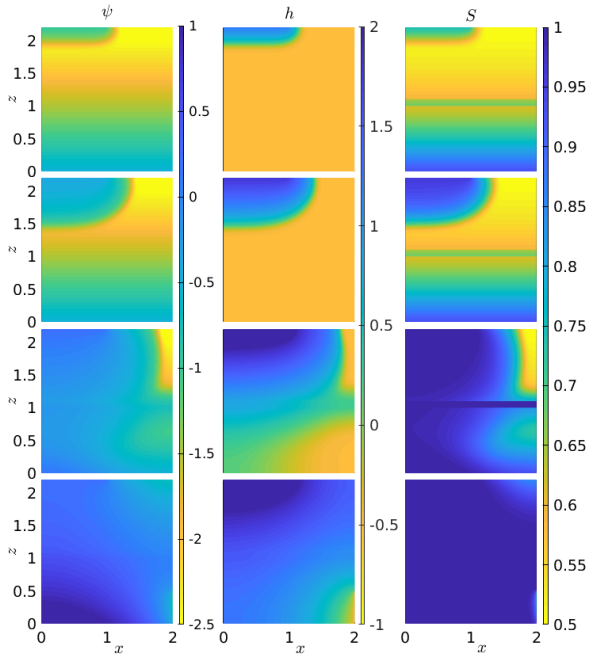

Figure 3: From left to right: pressure head ψ, hydraulic head $h = \psi + z$, and saturation S after 1, 2, 3, and 4 days (from top to bottom), where the fracture width is $l = 10$ *cm*, *fracture*: Hygiene sandstone, *solid matrix*: Guelph loam

right boundary. Then, the outflow increases by several orders of magnitude over the next day and is sustained as the solution is approaching a stationary state. Whereas the outflow in Effective model IV is in good agreement with the full model, in particular for a very thin fracture of width 1 cm, Effective model I predicts a later point in time for the fluid to pass through the fracture, and the total outflow remains too low until a stationary flow establishes after approximately four days. This is due to the storage term in the one-dimensional Richards equation that causes the fracture to fill up with water and delays the saturation process of the lower matrix block, which is unphysical since the storage capacity of the two-dimensional fracture is negligible given its small width. Finally, we remark that the outflow rate in Effective model III is similar to the one in Effective model I.

5.2. Impermeable fracture

Next, we consider the case that the fracture is much less permeable than the surrounding matrix blocks. For this purpose, we take the van Genuchten parameters for the fracture corresponding to sample 4030 in the UNSODA database and opt for Touchet silt loam as the solid matrix. This implies a saturated permeability ratio of $\sim 1 : 261$ between the fracture and the solid matrices. Now, we consider fractures of width 20 cm and 10 cm. For this choice, we have $\kappa \approx 0.053, 0.041$ and $\lambda \approx 2.42, 1.86$ for

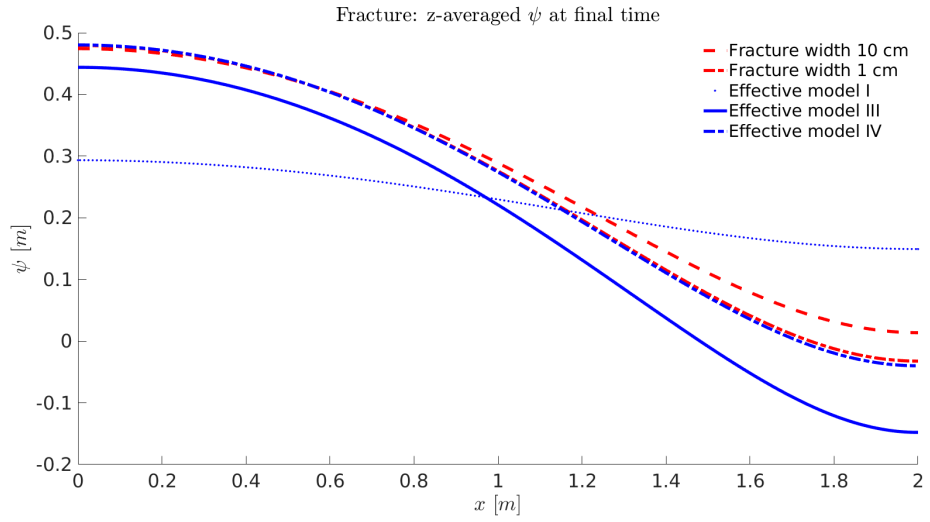

Figure 4: z-averaged pressure head in the fracture at final time $T = 4$ d, *fracture*: Hygiene sandstone, *solid matrix*: Guelph loam

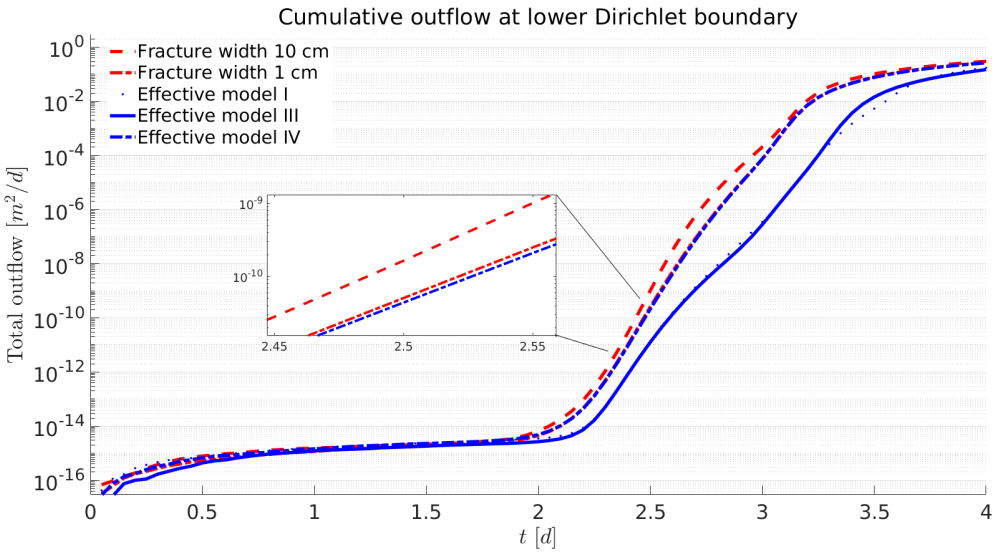

Figure 5: Cumulative outflow at lower Dirichlet boundary over time, *fracture*: Hygiene sandstone, *solid matrix*: Guelph loam

$l = 20\ cm, 10\ cm$, respectively. Accordingly, theory predicts Effective model VII* to be the appropriate choice for these soil properties and we anticipate that a steep pressure gradient across the fracture will form.

The simulations were run until an end time of $T = 0.2\ d$ at a time step of $\Delta t = 0.001\ d \approx 86\ s$. This means that at the final time of the simulation, the reservoir is still in the process of being filled.

Figure 6 shows the z-averaged pressure head at final time. Here, we compare the solution of the full model with Effective models I and IV as examples of effective models with continuous pressure at the fracture. Note that in Effective model VII* no pressure is defined in the fracture for which reason no curve for this effective model is depicted. One clearly sees that the average pressure along the fracture in the full models is much lower than in Effective models I and IV. The reason for this is that the inflowing water has not yet penetrated large parts of the fracture in the full models at the simulation end time; hence, the lower part of the fracture is unaffected by the inflow and remains at a low pressure. For the 20 cm wide fracture, larger parts of the fracture have not been in contact with the inflowing water as compared to the 10 cm wide fracture, which explains why the z-averaged pressure is lower in the former case. On the other hand, the continuous effective models do not impede the crossing of water through the fracture and the subsequent flow into the lower solid matrix. Consequently, the pressure profiles in the fracture do not resemble the ones of the full models at all, which is not surprising recalling that the theoretical part of this work predicts that this situation falls within the range of an effective model with discontinuous pressure at the interface.

Looking at the outflow at the lower Dirichlet boundary (see Figure 7) reveals that the no-flow interface condition in Effective model VII* is evidently the correct approximation for the two-dimensional fractures in the full model, for which the outflow lies within the range of machine accuracy. In contrast, in the continuous models, water leaves the domain after short time. To summarise this case, the simulation confirms our theoretical prediction that we are within the range of Effective model VII*, whereas continuous effective models would give a completely wrong description of the flow.

5.3. Permeable fracture

Let us now turn towards a case where the fracture is more conductive than the solid matrices. To be precise, we consider a fracture filled with Touchet silt loam, surrounded by solid matrix blocks of silt loam. For this constellation, the fracture is ~ 61 times as conductive as the matrix blocks when being fully saturated. Consequently, we expect that the flow along the fracture is substantial even for thin fractures. We consider fracture widths of $l = 10\ cm$ and $l = 1\ cm$ and choose $T = 4\ d$, $\Delta t = 0.05\ d$.

This yields $\kappa \approx -0.056, -0.032$ and $\lambda \approx -1.37, -0.78$ for $l = 10\ cm, 1\ cm$, respectively, implying that we expect the source term to vanish. Let us remark that this is typical in many common situations in subsurface flow where the porosities of the materials are within an order of magnitude. The situation for the flux term is less trivial. Since λ is close to minus one, Effective model II might be a good choice. For the 1 cm thick fracture, λ lies between -1 and 0 and thus, Effective model IV potentially approximates the full model well, too, while for the 10 cm thick fracture, λ is slightly smaller than minus one, which might hint at Effective model IX.

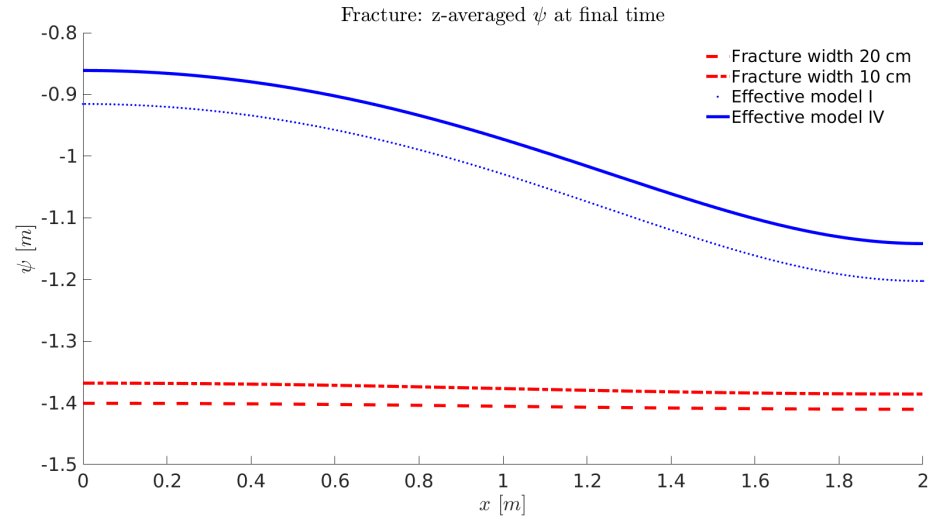

Figure 6: z-averaged pressure head in the fracture at final time $T = 0.2$ d, *fracture*: UNSODA sample 4030, *solid matrix*: Touchet silt loam

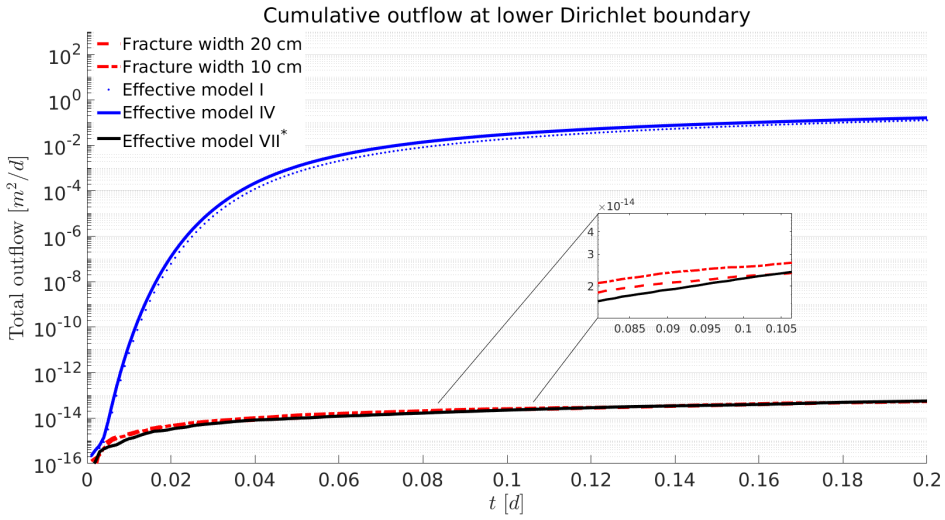

Figure 7: Cumulative outflow at lower Dirichlet boundary over time, *fracture*: UNSODA sample 4030, *solid matrix*: Touchet silt loam

Figure 8 shows the z-averaged pressure head at final time. We compare the solution of the full models to Effective models I, II, IV, and IX. The solutions of the full model

lie between the solution of Effective models II and IV, with Effective model II being a better approximation for the fracture of 10 cm width and Effective model IV being closer to the solution in case of a 1 cm wide fracture. This can be understood as follows: in the case of the thicker fracture, the fracture possesses enough volume to transport the inflowing water quickly to the right hand side of the domain, yielding a small pressure gradient along the fracture. As the fracture width decreases, less water can flow along the fracture causing the pressure gradient to rise. Effective model IV corresponds to the limit case where flow along the fracture no longer takes place, whereas the elliptic partial differential equation for the fracture in Effective model II expresses that inflowing water is distributed along the fracture without the fracture being able to store it. Clearly, the solutions of the full model interpolate between these two limit cases. In Effective model IX, which is suitable in a situation where the fracture permeability is much higher than the one in the solid matrices (i.e. $\lambda < -1$), the pressure in the fracture is spatially constant. At final time, this constant pressure is almost identical to the solution of Effective model II. Effective model I gives a poor approximation of the pressure in the fracture since the storage term of the one-dimensional Richards equation is too big as compared to the one of the two-dimensional thin fractures.

Figure 9 shows the cumulative outflow across the lower right domain boundary over time. Effective model IX is not a suitable approximation in this situation as inflow on the left hand side of the fracture is instantaneously distributed along the entire fracture which causes the water to reach the lower right domain boundary much earlier than in the full models. This is despite the fact that for $l = 10\ cm$, we have $\lambda < -1$, showing that leaving out higher order terms can lead to severe errors and that convergence is only obtained in the limit of vanishing fracture width. In Effective model II, the outflow increases earlier than in Effective models I and IV due to the quick transport of water along the fracture without any storage, which gives a good approximation of the outflow of the full model with a fracture of width 10 cm. Thus, Effective model II, corresponding to $\kappa > -1$, $\lambda = -1$, gives the best approximation here, which fits well the actual parameters $\kappa \approx -0.056$, $\lambda \approx -1.37$. In contrast, the outflow of water rises slower in Effective model IV since there is no flux term in the fracture. The outflow in the full model with a fracture of 1 cm width lies in between Effective models II and IV as expected due to $\lambda \approx -0.78$. After four days, the total outflow is very similar in all models except for Effective model I, where the outflow through the domain boundary is reduced since parts of the water can be stored in the fracture.

From this example, it can be seen that in many realistic situations, it is not trivial to determine which effective model is the right one since the upscaled model is only obtained in the limit. Besides, it illustrates the need for higher order correction terms that account for the non-zero fracture width.

6. Conclusion

We have developed effective equations for replacing a fracture by an interface for Richards' equation. The starting geometry is a fracture of small thickness ε in a porous medium. The effective models are derived as the limit of $\varepsilon \to 0$. The ratios of porosity and absolute permeability of the fracture and the porous matrix are characterised by ε^κ and ε^λ, respectively. The effective equations depend on the two parameters κ and λ and

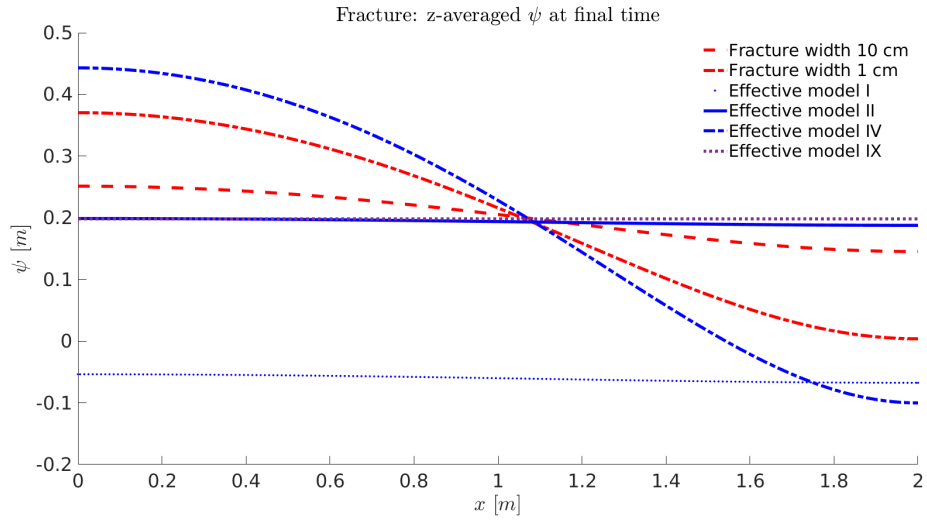

Figure 8: z-averaged pressure head in the fracture at final time $T = 4$ d, *fracture*: Touchet silt loam, *solid matrix*: silt loam

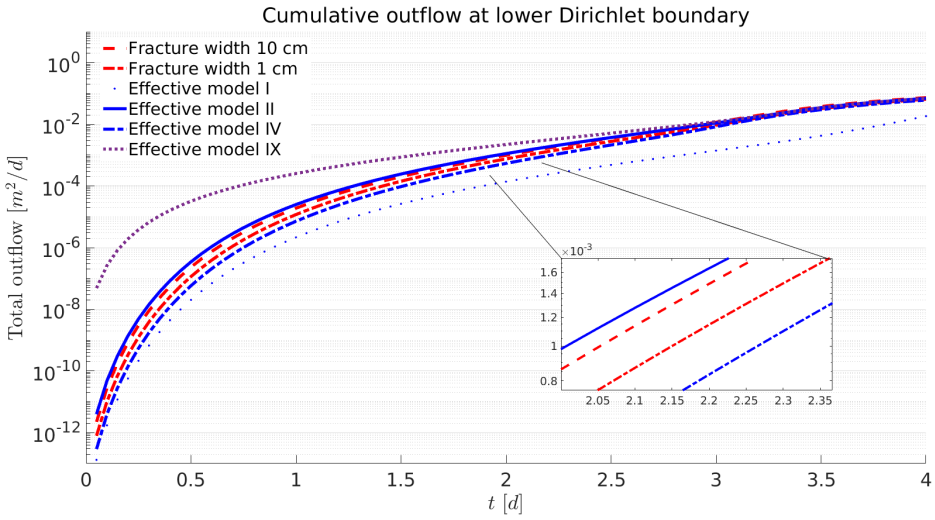

Figure 9: Cumulative outflow at lower Dirichlet boundary over time, *fracture*: Touchet silt loam, *solid matrix*: silt loam

we cover the cases $\kappa \geq -1, \lambda \in (-\infty, \infty)$. The numerical examples show that the upscaled models approximate the ε problem in a satisfactory manner. Further exploration

of the numerical tests for the different upscaled models will be carried out elsewhere.

7. Acknowledgements

The work of K. Kumar and F. A. Radu was partially supported by the Research Council of Norway through the projects Lab2Field no. 811716, IMMENS no. 255426, CHI no. 25510 and Norwegian Academy of Science and Statoil through VISTA Ada-Sim no. 6367. I. S. Pop was supported by the Research Foundation-Flanders (FWO) through the Odysseus programme (project GOG1316N) and by Statoil through the Akademia agreement.

References

[1] P. Adler, J. Thovert, *Fractures and Fracture Networks*, Theory and Applications of Transport in Porous Media, Springer, 1999.

[2] J. Aghili, K. Brenner, J. Hennicker, R. Masson, L. Trenty, *Two-phase Discrete Fracture Matrix models with linear and nonlinear transmission conditions*, hal-01764432v1, https://hal.archives-ouvertes.fr/hal-01764432v1, 2018.

[3] E. Ahmed, J. Jaffré, J. E. Roberts, *A reduced fracture model for two-phase flow with different rock types*, Mathematics and Computers in Simulation 137: 49-70, 2017.

[4] H. Alt, S. Luckhaus, and A. Visintin, *On nonstationary flow through porous media*, Ann. Mat. Pura Appl. 136: 303–316, 1984.

[5] P. Ø. Andersen, S. Evje, *A model for reactive flow in fractured porous media*, Chemical Engineering Science 145: 196–213, 2016.

[6] T. Arbogast, M. F. Wheeler, N. Y. Zhang, *A non-linear mixed finite element method for a degenerate parabolic equation arising in flow in porous media*, SIAM J. Numer. Anal. 33: 1669–1687, 1996.

[7] T. Arbogast, L. C. Cowsar, M. F. Wheeler, and I. Yotov, *Mixed finite element methods on nonmatching multiblock grids*, SIAM Journal on Numerical Analysis, 37(4), 1295-1315, 2000.

[8] H. Berninger, R. Kornhuber, O. Sander, *A multidomain discretization of the Richards equation in layered soil*, Comput. Geosci. 19 (1): 213–232, 2015.

[9] I. Berre, F. Doster, E. Keilegavlen, *Flow in fractured porous media: A review of conceptual models and discretization approaches*, Transport in Porous Media,1-22, 2018.

[10] W. M. Boon, J. M. Nordbotten, I. Yotov, *Robust discretization of flow in fractured porous media*, SIAM Journal on Numerical Analysis, 56(4), 2203–2233, 2018.

[11] M. Bukac, I. Yotov, P. Zunino, *Dimensional model reduction for flow through fractures in poroelastic media*, ESAIM: Mathematical Modelling and Numerical Analysis 51(4): 1429–1471, 2017.

[12] C. Cancès, M. Pierre, *An existence result for multidimensional immiscible two-phase flows with discontinuous capillary pressure field*, SIAM J. Math. Anal. 44(2): 966–992, 2012.

[13] M. A. Celia, E. T. Bouloutas, R. L. Zarba, *A general mass–conservative numerical solution for the unsaturated flow equation*, Water resources research 26.7: 1483-1496, 1990.

[14] C. J. van Duijn, L. A. Peletier, *Nonstationary filtration in partially saturated porous media*, Arch. Rational Mech. Anal. 78: 173–198, 1982.

[15] M. Karimi-Fard, L. J. Durlofsky, K. Aziz, *An efficient discrete-fracture model applicable for general-purpose reservoir simulators*, SPE J. 9: 227–236, 2004.

[16] C. Ebmeyer, *Error estimates for a class of degenerate parabolic equations*, SIAM J. Numer. Anal. 35: 1095–1112, 1998.

[17] M. F. El-Amin, A. Salama, and S. Sun, *Numerical and dimensional analysis of nanoparticles transport with two-phase flow in porous media*, Journal of Petroleum Science and Engineering 128: 53-64, 2015.

[18] R. Eymard, M. Gutnic, D. Hilhorst, *The finite volume method for Richards equation*, Comput. Geosci. 3: 259–294, 1999.

[19] R. Eymard, D. Hilhorst, M. Vohralík, *A combined finite volume-nonconforming/mixed-hybrid finite element scheme for degenerate parabolic problems*, Numer. Math. 105: 73–131, 2006.

[20] A. Ferroni, L. Formaggia, A. Fumagalli, *Numerical analysis of Darcy problem on surfaces* ESAIM: Mathematical Modelling and Numerical Analysis, 50(6): 1615–1630, 2016.

[21] A. Fumagalli, E. Keilegavlen, S. Stefano, *Conforming, non-conforming and non-matching discretization couplings in discrete fracture network simulations*, Journal of Computational Physics 376: 694-712, 2019.

[22] M. Th. van Genuchten, *A closed-form equation for predicting the hydraulic conductivity of unsaturated soils*, Soil Sci. Soc. Am. J., 44: 892–898, 1980.

[23] V. Girault, K. Kumar, and M. F. Wheeler, *Convergence of iterative coupling of geomechanics with flow in a fractured poroelastic medium*, Comp. Geosciences, 20(5): 997–1011, 2016.

[24] V. Girault, M. F. Wheeler, K. Kumar, G. Singh, *Mixed Formulation of a Linearized Lubrication Fracture Model in a Poro-elastic Medium*, Contributions to Partial Differential Equations and Applications, Springer, Cham, 171–219, 2019.

[25] D. Gläser, R. Helmig, B. Flemisch, H. Class, *A discrete fracture model for two-phase flow in fractured porous media*, Adv. Water Resour. 110: 335-348, 2017.

[26] R. Helmig, *Multiphase flow and transport processes in the subsurface: a contribution to the modeling of hydrosystems*, Springer-Verlag, 1997.

[27] H. Hoteit, A. Firoozabadi, *Numerical modeling of diffusion in fractured media for gas injection and recycling schemes*, SPE Annual Technical Conference and Exhibition, Society of Petroleum Engineers, 2006.

[28] E. Hough, J. M. Pearce, S. J. Kemp, G. M. Williams, *An investigation of some sediment-filled fractures within redbed sandstones of the UK*, Proceedings of the Yorkshire Geological Society 56: 41–53, 2006.

[29] W. Jäger, J. Kačur, *Solution of porous medium type systems by linear approximation schemes*, Numerische Mathematik 60, 1: 407-427, 1991.

[30] R. A. Klausen, F. A. Radu, G. T. Eigestad, *Convergence of MPFA on triangulations and for Richards' equation*, Int. J. Numer. Meth. Fluids 58: 1327–1351, 2008.

[31] M. Karimi-Fard, A. Firoozabadi, *Numerical simulation of water injection in 2D fractured media using discrete-fracture model*, SPE annual technical conference and exhibition, Society of Petroleum Engineers, 2011.

[32] F. J. Leij, W. J. Alves, M. T. van Genuchten, J. R. Williams, *The UNSODA unsaturated soil hydraulic database*, in: M. T. van Genuchten, F. J. Leij, L. Wu., eds. Characterization and measurement of the hydraulic properties of unsaturated porous media. University of California, Riverside, CA, USA, 1269–1281, 1999.

[33] P. L. Lions, *On the Schwarz alternating method. III: a variant for nonoverlapping subdomains*, Third international symposium on domain decomposition methods for partial differential equations, Vol. 6, 202–223, SIAM Philadelphia, PA, 1990.

[34] F. List, *Upscaling of Richards' Equation in Fractured Porous Media*, Master Thesis, TU Eindhoven, 2017.

[35] F. List, F. A. Radu, *A study on iterative methods for solving Richards' equation*, Comput. Geosci. 20(2): 341–353, 2016.

[36] F. List, K. Kumar, I. S. Pop, F. A. Radu. *Upscaling of unsaturated flow in fractured porous media*. arXiv preprint arXiv:1807.05993, 2018.

[37] V. Martin, J. Jaffré, J. E. Roberts, *Modeling fractures and barriers as interfaces for flow in porous media*, SIAM Journal on Scientific Computing 26(5): 1667-1691, 2005.

[38] F. Morales, R. E. Showalter, *The narrow fracture approximation by channeled flow*, Journal of Mathematical Analysis and Applications 365(1): 320-331, 2010.

[39] F. Morales, R. E. Showalter, *Interface approximation of Darcy flow in a narrow channel*, Mathematical Methods in the Applied Sciences 35(2): 182-195, 2012.

[40] I. Neuweiler, H. Eichel, *Restricted access effective parameter functions for the Richards equation in layered porous media*, Vadose Zone J. 5(3): 963–977, 2006.

[41] M. Neuss-Radu, W. Jäger, *Effective transmission conditions for reaction-diffusion processes in domains separated by an interface*, SIAM Journal on Mathematical Analysis 39(3): 687-720, 2007.

[42] R. H. Nochetto, C. Verdi, *Approximation of degenerate parabolic problems using numerical integration*, SIAM J. Numer. Anal. 25: 784–814, 1988.

[43] F. Otto, *L1-contraction and uniqueness for unstationary saturated-unsaturated porous media flow*, Adv. Math. Sci. Appl. 2: 537–553, 1997.

[44] I. S. Pop, J. Bogers, K. Kumar, *Analysis and upscaling of a reactive transport model in fractured porous media involving nonlinear transmission condition*, Vietnam J. Math. 45: 77–102, 2016.

[45] I. S. Pop, B. Schweizer, *Regularization schemes for degenerate Richards equations and outflow conditions*, Mathematical Models and Methods in Applied Sciences 21.08: 1685-1712, 2011.

[46] M. Peszyńska, M. F. Wheeler, I. Yotov, *Mortar upscaling for multiphase flow in porous media*, Computational Geosciences, 6(1), pp.73-100, 2002.

[47] P. Popov, G. Qin, L. Bi, Y. Efendiev, R. E. Ewing, J. Li, *Multiphysics and multiscale methods for modeling fluid flow through naturally fractured carbonate karst reservoirs*, SPE Reservoir Evaluation & Engineering 12, 02: 218-231, 2009.

[48] F. A. Radu, I. S. Pop, P. Knabner, *Order of convergence estimates for an Euler implicit, mixed finite element discretization of Richards' equation*, SIAM J. Numer. Anal. 42: 1452–1478, 2004.

[49] L. A. Richards, *Capillary conduction of liquids through porous mediums*, J. Appl. Phys. 1(5): 318–333, 1931.

[50] T. H. Sandve, I. Berre, J. M. Nordbotten, *An efficient multi-point flux approximation method for discrete fracture–matrix simulations*, Journal of Computational Physics, 231(9), 3784-3800, 2012.

[51] N. Schwenck, B. Flemisch, R. Helmig, B. I. Wohlmuth, *Dimensionally reduced flow models in fractured porous media: crossings and boundaries*, Comput. Geosci. 19: 1219–1230, 2015.

[52] E. Schneid, *Hybrid-Gemischte Finite-Elemente-Diskretisierung der Richards-Gleichung*, PhD Thesis (in German), University of Erlangen-Nürnberg, Germany, 2004.

[53] D. Seus, K. Mitra, I. S. Pop, F. A. Radu, C. Rohde, *A linear domain decomposition method for partially saturated flow in porous media*, Comput. Methods Appl. Mech. Engrg. 333: 331–355, 2018.

[54] M. Tene, S. B. M. Bosma, M. S. Al Kobaisi, H. Hajibeygi, *Projection-based embedded discrete fracture model (pEDFM)*, Advances in Water Resources 105, 205–216, 2017.

[55] X. Tunc, La modlisation des failles conductrices pour les coulements en milieux poreux, *PhD thesis*, Université De Provence, 2012.

[56] A. Mikelic, M. F. Wheeler, T. Wick, *A phase-field method for propagating fluid-filled fractures coupled to a surrounding porous medium*, SIAM Multiscale Modeling Simulation 13(1): 367–398, 2015.

[57] C. Woodward, C. Dawson, *Analysis of expanded mixed finite element methods for a non-linear parabolic equation modeling flow into variably saturated porous media*, SIAM J. Numer. Anal. 37: 701–724, 2000.

UHasselt Computational Mathematics Preprint Series

2019

UP-19-03 *K. Kumar, F. List, I.S. Pop, F.A. Radu*, **Formal upscaling and numerical validation of fractured flow models for Richards' equation**, 2019

UP-19-02 *M.A. Endo Kokubun, A. Muntean, F.A. Radu, K. Kumar, I.S. Pop, E. Keilegavlen, K. Spildo*, **A pore-scale study of transport of inertial particles by water in porous media**, 2019

UP-19-01 *Carina Bringedal, Lars von Wolff, and Iuliu Sorin Pop*, **Phase field modeling of precipitation and dissolution processes in porous media: Upscaling and numerical experiments**, 2019

2018

UP-18-09 *David Landa-Marbán, Gunhild Bodtker, Kundan Kumar, Iuliu Sorin Pop, Florin Adrian Radu*, **An upscaled model for permeable biofilm in a thin channel and tube**, 2018

UP-18-08 *Vo Anh Khoa, Le Thi Phuong Ngoc, Nguyen Thanh Long*, **Existence, blow-up and exponential decay of solutions for a porous-elastic system with damping and source terms**, 2018

UP-18-07 *Vo Anh Khoa, Tran The Hung, Daniel Lesnic*, **Uniqueness result for an age-dependent reaction-diffusion problem**, 2018

UP-18-06 *Koondanibha Mitra, Iuliu Sorin Pop*, **A modified L-Scheme to solve nonlinear diffusion problems**, 2018

UP-18-05 *David Landa-Marban, Na Liu, Iuliu Sorin Pop, Kundan Kumar, Per Pettersson, Gunhild Bodtker, Tormod Skauge, Florin A. Radu*, **A pore-scale model for permeable biofilm: numerical simulations and laboratory experiments**, 2018

UP-18-04 *Florian List, Kundan Kumar, Iuliu Sorin Pop and Florin A. Radu*, **Rigorous upscaling of unsaturated flow in fractured porous media**, 2018

UP-18-03 *Koondanibha Mitra, Hans van Duijn*, **Wetting fronts in unsaturated porous media: the combined case of hysteresis and dynamic capillary**, 2018

UP-18-02 *Xiulei Cao, Koondanibha Mitra*, **Error estimates for a mixed finite element discretization of a two-phase porous media flow model with dynamic capillarity**, 2018

UP-18-01 *Klaus Kaiser, Jonas Zeifang, Jochen Schütz, Andrea Beck and Claus-Dieter Munz*, **Comparison of different splitting techniques for the isentropic Euler equations**, 2018

2017

UP-17-12 *Carina Bringedal, Tor Eldevik, Øystein Skagseth and Michael A. Spall*, **Structure and forcing of observed exchanges across the Greenland-Scotland Ridge**, 2017

UP-17-11 *Jakub Wiktor Both, Kundan Kumar, Jan Martin Nordbotten, Iuliu Sorin Pop and Florin Adrian Radu*, **Linear iterative schemes for doubly degenerate parabolic equations**, 2017

UP-17-10 *Carina Bringedal and Kundan Kumar*, **Effective behavior near clogging in upscaled equations for non-isothermal reactive porous media flow**, 2017

UP-17-09 *Alexander Jaust, Balthasar Reuter, Vadym Aizinger, Jochen Schütz and Peter Knabner*, **FESTUNG: A MATLAB / GNU Octave toolbox for the discontinuous Galerkin method. Part III: Hybridized discontinuous Galerkin (HDG) formulation**, 2017

UP-17-08 *David Seus, Koondanibha Mitra, Iuliu Sorin Pop, Florin Adrian Radu and Christian Rohde*, **A linear domain decomposition method for partially saturated flow in porous media**, 2017

UP-17-07 *Klaus Kaiser and Jochen Schütz*, **Asymptotic Error Analysis of an IMEX Runge-Kutta method**, 2017

UP-17-06 *Hans van Duijn, Koondanibha Mitra and Iuliu Sorin Pop*, **Travelling wave solutions for the Richards equation incorporating non-equilibrium effects in the capillarity pressure**, 2017

UP-17-05 *Hans van Duijn and Koondanibha Mitra*, **Hysteresis and Horizontal Redistribution in Porous Media**, 2017

UP-17-04 *Jonas Zeifang, Klaus Kaiser, Andrea Beck, Jochen Schütz and Claus-Dieter Munz*, **Efficient high-order discontinuous Galerkin computations of low Mach number flows**, 2017

UP-17-03 *Maikel Bosschaert, Sebastiaan Janssens and Yuri Kuznetsov*, **Switching to nonhyperbolic cycles from codim-2 bifurcations of equilibria in DDEs**, 2017

UP-17-02 *Jochen Schütz, David C. Seal and Alexander Jaust*, **Implicit multiderivative collocation solvers for linear partial differential equations with discontinuous Galerkin spatial discretizations**, 2017

UP-17-01 *Alexander Jaust and Jochen Schütz*, **General linear methods for time-dependent PDEs**, 2017

2016

UP-16-06 *Klaus Kaiser and Jochen Schütz*, **A high-order method for weakly compressible flows**, 2016

UP-16-05 *Stefan Karpinski, Iuliu Sorin Pop, Florin A. Radu*, **A hierarchical scale separation approach for the hybridized discontinuous Galerkin method**, 2016

UP-16-04 *Florin A. Radu, Kundan Kumar, Jan Martin Nordbotten, Iuliu Sorin Pop*, **Analysis of a linearization scheme for an interior penalty discontinuous Galerkin method for two phase flow in porous media with dynamic capillarity effects** , 2016

UP-16-03 *Sergey Alyaev, Eirik Keilegavlen, Jan Martin Nordbotten, Iuliu Sorin Pop*, **Fractal structures in freezing brine**, 2016

UP-16-02 *Klaus Kaiser, Jochen Schütz, Ruth Schöbel and Sebastian Noelle*, **A new stable splitting for the isentropic Euler equations**, 2016

UP-16-01 *Jochen Schütz and Vadym Aizinger*, **A hierarchical scale separation approach for the hybridized discontinuous Galerkin method**, 2016